Ocean Engineering 330 (2025) 121235

Contents lists available at ScienceDirect

Ocean Engineering

journal homepage: www.elsevier.com/locate/oceaneng

Research paper

Advancements in mooring systems for the OE35 wave energy converter: Dynamic design and validation

Chenyu Zhao [a,*], Faryal Khalid [b], Tony Lewis [c], Sean Barrett [c], Brian McSwiney [c], Rémy CR. Pascal [d], Bernardo Kahn [d], Lars Johanning [a]

[a] University of Plymouth, United Kingdom
[b] University of Exeter, United Kingdom
[c] Ocean Energy, Ireland
[d] Innosea, France

ARTICLE INFO

Keywords:
OE35
Wave energy converter
Mooring
Orcaflex
Tank test

ABSTRACT

This research presents a comprehensive analysis of the mooring system design for the 1 MW OE35 wave energy converter, which is being developed by the WEDUSEA project. The study centres on the dynamic analysis of mooring configurations using Orcaflex software to simulate the environmental and operational conditions expected at the deployment site. The analysis involved an iterative design and validation process, refined through both numerical modelling and basin testing. These tank tests were crucial for validating the Orcaflex model outcomes by providing a controlled environment to observe the physical behaviours of the proposed mooring configurations under simulated sea conditions. The finalized mooring system design employs a three-point catenary setup, optimized through extensive simulation to withstand varied environmental loads while maintaining system integrity and device stability. This paper outlines the progression from initial mooring concepts to a thoroughly validated design, demonstrating improvements in mooring strategies that enhance the reliability and performance of wave energy converters in real sea conditions. The findings from this analysis contribute significantly to the ongoing efforts to scale wave energy technologies, aligning with broader industry targets for cost reduction and sustainability in renewable energy deployments.

1. Introduction

Wave energy converters (WECs) harness the kinetic and potential energy generated by the movement of ocean waves, representing a promising and largely untapped source of renewable energy (Clemente et al., 2021; Jin and Greaves, 2021). Among the various technologies explored for wave energy conversion, the Oscillating Water Column (OWC) stands out due to its simplicity and effectiveness (Kushwah, 2021). OWC devices convert wave motion into a stream of high-velocity air, driving a turbine connected to a generator (Czech and Bauer, 2012). Traditionally, these systems have been installed onshore or as part of fixed structures, but recent advances have seen the development of floating OWC systems, which can be deployed offshore in deeper waters where wave energy is more abundant (Vannucchi and Cappietti, 2016).

Floating OWCs offer several advantages over their fixed counterparts, primarily due to their ability to operate in deeper waters with higher wave energy potential. Unlike fixed systems that are limited to shallow waters, floating OWCs can be positioned in more energetic wave regimes, significantly increasing energy capture efficiency (Gomes et al., 2011). A study by Kisacik et al. (2020) highlights the efficiency and survivability of floating OWCs moored to the seabed, emphasizing their capability to harness wave energy in various ocean conditions.

Some other floating OWC would benefit from a stable platform, such as integrating with floating offshore wind turbines (FOWTs), This design can transform these structures into multi-purpose platforms that harness both wind and wave energies. This integration not only improves the structural response and stability of the FOWT but also enhances the overall energy output by utilizing complementary airflow control strategies (Aubault et al., 2011; M'zoughi et al., 2021; Zhou et al., 2020).

Despite the numerous advantages, floating OWCs face significant challenges, particularly in their mooring systems. The dynamic environment of the ocean can lead to substantial loads on the mooring lines, which must be robust enough to prevent failure but also flexible enough to avoid over-restraining the floating structure. This balance is critical to

* Corresponding author.
E-mail address: chenyu.zhao@plymouth.ac.uk (C. Zhao).

https://doi.org/10.1016/j.oceaneng.2025.121235
Received 8 October 2024; Received in revised form 21 March 2025; Accepted 11 April 2025
Available online 15 April 2025

ensure the longevity and effectiveness of the floating OWC. Khaleghi et al. (2022) discuss the complexities involved in designing mooring systems for floating OWCs, highlighting that these systems must balance the need for stability with the flexibility to adapt to varying sea conditions. Another study emphasised the influence of incident wave angles on the device's motions. The control of mooring restoring force by forward mooring lines is essential to ensure stability and optimal performance (Pols et al., 2021).

Given the challenges, a comprehensive design approach for the mooring system is essential to the successful deployment and operation of floating OWCs. A well-designed mooring system not only ensures the structural integrity and operational efficiency of the OWC but also plays a crucial role in the economic viability of the project. In last 10 years, significant progresses have been obtained in the area of floating OWC mooring design. For example, Freeman et al. (2014) emphasize the need for advanced modelling and simulation techniques to predict the behaviour of mooring systems under various ocean conditions. These techniques can help optimize the design parameters, such as the type of mooring lines, their length, and the anchoring methods, to achieve a reliable and cost-effective solution. Moreover, incorporating redundancy into the mooring design can enhance the resilience of the system, reducing the risk of catastrophic failures. Gubesch et al. (2022) presented a systematic experimental investigation of a 1:36 scale OWC WEC model. It was tested in fixed, free-floating, and moored conditions with three mooring configurations: tension leg, 45° taut, and catenary mooring with heavy chains. The study analysed capture width ratios (CWR), response amplitude operators, mooring tensions, and turbine damping coefficients. Results showed that the 45° taut mooring performed best, with significant mooring tensions correlating with increased CWRs, while heave motions contributed to power absorption for taut moorings. Another experimental study (Xu et al., 2020), focused on a traditional OWC chamber and a Backward Bend Duct Buoy (BBDB) chamber which moored three flexible mooring systems. The study found significant nonlinearities in mooring tension, especially in low wave period conditions. Surge and yaw motions varied significantly with different mooring systems.

Many previous studies have focused on smaller-scale or initial design phase devices that may not be fully suitable for real sea conditions or budget constraints. This paper dynamically and comprehensively designs the mooring system for the 1 MW OE35 OWC device. Developed by Irish company New Wave Technologies Ltd trading as "OceanEnergy" (OE), the OE35 is recognized as the world's largest capacity floating wave energy device (OceanEnergy, 2024). Operating on a simple yet effective principle, the OE35 is anchored to the ocean floor and features three large airtight chambers. As waves rise and fall, they drive air in and out of these chambers, powering a turbine to generate electricity. The mooring design proposed in this paper will be implemented in further demonstrations and testing of the OE35 at the European Marine Energy Centre (EMEC) (EMEC, 2023) in Orkney, Scotland.

The remainder of this paper is structured as follows: Section 2 introduces the comprehensive mooring design approach for the OE35 prototype, encompassing both numerical simulations and scaled tank testing. Section 3 presents the results derived from this design approach and details the finalized mooring configuration for the OE35 prototype. Section 4 summarizes the main findings and contributions of this study.

2. Mooring design approach

This paper comprehensively outlines a three-stage mooring design methodology for the OE35, including: a. Conduct multiple mooring simulations to determine the maximum mooring line loads for full-scale deployment and to obtain the horizontal stiffness of the whole system; b. Validate and refine the results through scaled tank testing, using the time history data from phase a, focusing on the scenario with the highest tension; c. Using the most validated case from phase b, perform additional simulations to identify the maximum resultant tension for the full-scale device.

2.1. OE 35 device

The OE35, is categorized as a barge-type floater within a backward bent duct buoy configuration, representing a specific subset of OWC. An illustrative rendering of the OE35 design is provided in Fig. 1. Table 1 details the primary characteristics of the OE35, along with the sources of the respective information. The centre of gravity for both the equipment and PTO is assumed to coincide with that of the steel lightship, due to the proximity of the equipment's location to the lightship's centre of gravity. In this paper, the machinery onboard had not been comprehensively defined; however, this approximation was considered acceptable since the total machinery weight constitutes a minor percentage of the overall weight. Additional details of the OE35 can be found in (Johanning, 2023).

2.2. Design load case

To engineer a design capable of withstanding the most severe wave conditions, the DLC 6.1 is formulated to represent a survival scenario in which the PTO is either parked or idling (INNOSEA, 2022). This particular DLC (defined by JONSWAP spectrum) involves a rigorous simulation of an extreme stochastic sea state over a 3-h duration, designed to reflect conditions with a 10-year return period For short-term deployment of a WEC, the return period of environmental loads can be taken as five times the short-term deployment operational life, with a minimum of five years and a maximum of fifty years. Considering that for the WEDUSEA project, the deployment period will be of two years, the return periods of the environmental loads in this task were adjusted accordingly, following the recommendations from the IEC (Commission, 2021). Additionally, it includes the application of extreme current loads, characterized by a constant current speed representative of a 5-year return period, and extreme constant wind speeds, also based on a 5-year return period. The scenario further accounts for significant variations in water levels.

The weather data in this paper is based on information provided by EMEC and data extracted from the ResourceCode (INNOSEA, 2022) database from the past 20 years. ResourceCode was used in preference to EMEC data, because there was not sufficient data and its location was well away from the deployment site. Fig. 2 highlights in red the point 250070 from the ResourceCode database where data was extracted from, at the West coast of Orkney and Fig. 3 shows the location of the data point in relation to the OE35 location at EMEC.

Extreme value analysis was performed with the sea state conditions presented by the ResourceCode (INNOSEA, 2022), the GPD method was applied with a threshold. The toolbox and default GPD parameters

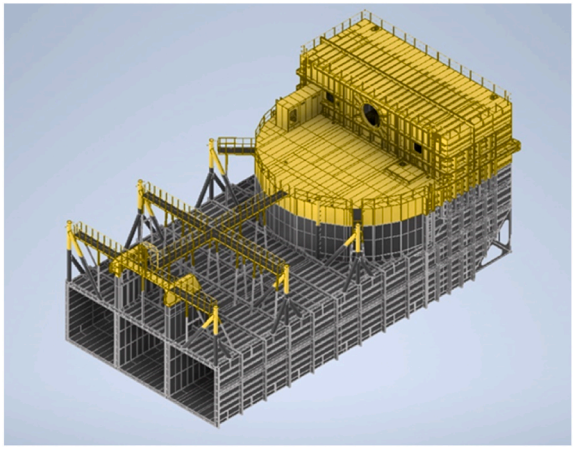

Fig. 1. Overview of the OE35 prototype design.

Table 1
Main characteristics of OE35 prototype.

Parameter	Value
Floater Draft (m)	8
Length Overall (m)	37.40
Breadth (m)	18.49
Depth at top of superstructure (m)	20.30
Centre of Gravity of steel lightship (m)	(4.436,-0.020,-3.144)
Mass of equipment and PTO (ton)	21.25

provided by ResourceCode to perform the analysis are used. The output of the extreme values analyses included different combinations of the wave periods and heights under different wave directions. However, considering the main scope of this paper, Table 2 just listed the final selection of the extreme weather conditions used in the mooring design. All details of analysis process can be found in (INNOSEA, 2022).

The wind model utilized features a turbulent field, while the current model is based on a constant speed, incorporating variations in water depth. Both wind and current directions are aligned with the wave headings in the DLC, ensuring that the interactions between these environmental factors are coherently represented in the survival condition simulation.

2.3. Design criteria

The mooring design criteria applied in this task was based on the recommendations of the IEC-TS 62600-10 (Commission, 2021) standard and the reference standard from DNV-GL for mooring design DNVGL-OS-E301 (DNV, 2018). The following procedure is followed to calculate the design tension.

$$T_d = \gamma T_{sim} \quad (1)$$

Where:

T_{sim}: total mooring tensions extracted from the simulations;

γ: safety factor, 1.67 in for DLC 6.1 in this paper (This assumption was made since the device is deployed at a secured test site, unmanned

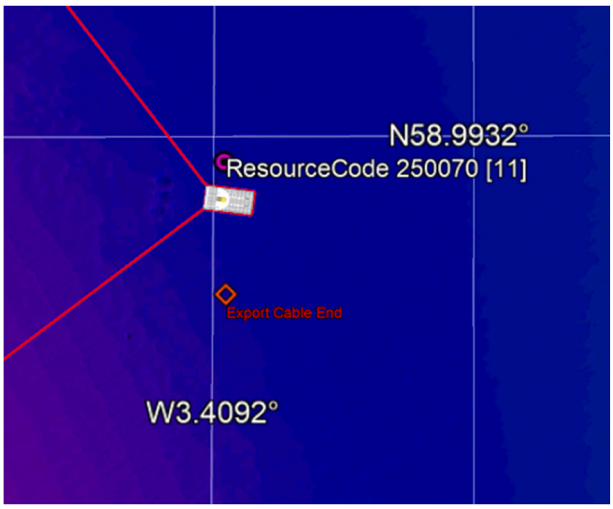

Fig. 3. Location of Data Reference Point 250070 in relation to OE35 at EMEC.

Table 2
Main characteristics of DLC 6.1 (INNOSEA, 2022).

Load	DLC 6.1
Wind (m/s)	24.91
Current (m)	0.77
Significant wave height (m)	12.93
Peak wave period (s)	15

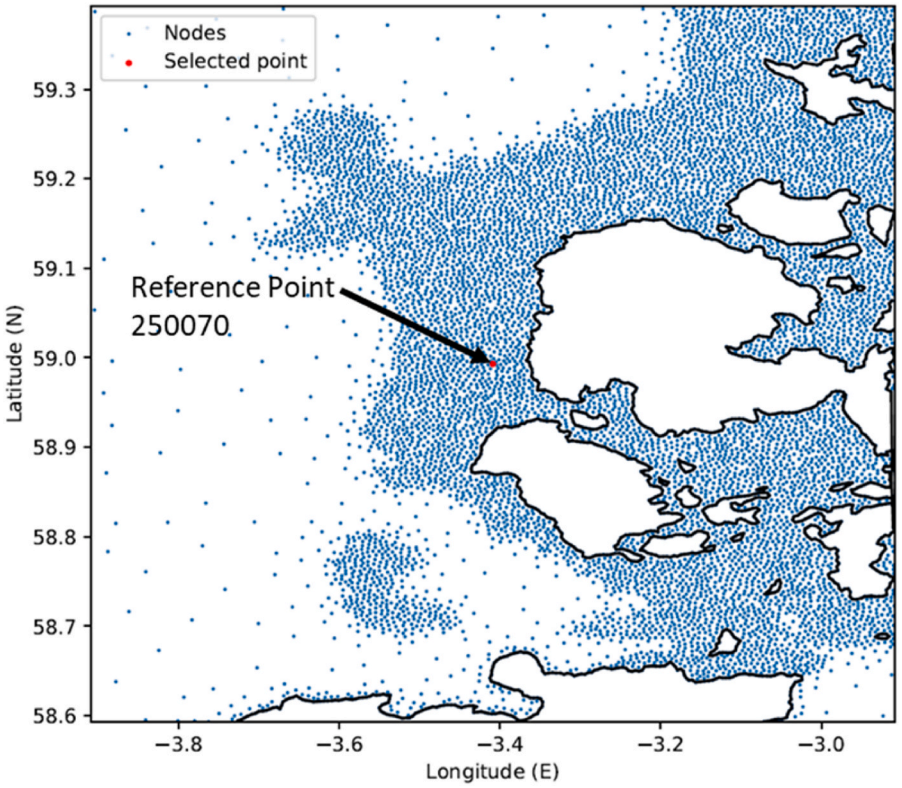

Fig. 2. Location of point 250070 used to extract data (in red), West coast of Orkney. (For interpretation of the references to colour in this figure legend, the reader is referred to the Web version of this article.)

and without dangerous cargo).

The design criterion can be defined as:

$$0.95MBL > T_d \tag{2}$$

Where:

MBL: minimum breaking load of the mooring line, coming from supplier catalogues [kN];

T_d: design tension, the tension experienced by the mooring lines.

2.4. Orcaflex simulation

2.4.1. OE 35 modelling

The numerical approach, including both frequency-domain and time-domain modules, has been used in other authors' studies (Wang et al., 2022; Zhao et al., 2023). As presented in Fig. 4, the hydrodynamic coefficients of the OE35 are calculated by a frequency-domain solver, OrcaWave. The nonlinear forces, such as the mooring loads, will be considered in the time domain with a solver known as the OrcaFlex (Orcina, 2024).The output of this time-domain module includes the Hydrodynamic Response of the device tensile load of the mooring system.

Based on recommendations from Orcawave, the mesh design for the OE35 platform did not include appendages due to their sharp edges, which could potentially lead to an overestimation of second order loads. This is akin to pruning a tree to prevent overgrowth—by removing these elements, the analysis becomes more manageable and accurate. However, to ensure that the influence of these components was still considered, Morison elements were incorporated into the simulation. These elements allow for the inclusion of drag forces in the computation of the displacement Response Amplitude Operators (RAOs), functioning much like adding weights to a scale to measure the impact indirectly. OrcaWave's software capabilities extend to linearizing quadratic loads, which is somewhat like simplifying a complex equation to understand its components better. This process is crucial for evaluating their effects not only on displacement RAOs but also on wave drift forces, providing a clearer picture of how the OE35 platform would behave under various sea conditions.

The OE35 was conceptualized as a barge-type structure in this paper, which means the consideration of the mass of water that could potentially be trapped within the device is considered. It was assumed for these calculations that the entire inner space of the device was filled with water, a detail that is specifically noted as "Trapped Water" in Table 3. This inclusion is critical for assessing the stability and dynamic responses of the OE35 under various operational condition.

Table 3
Mass and inertia of OE35.

	Mass [Te]	Ixx [Te. m^2]	Iyy [Te. m^2]	Izz [Te. m^2]
Lightship steel + equipment + Ballast	720.12	5.62e5	5.36e5	7.05e3
Trapped water	3790.85	2.29e5	5.45e5	5.46e6
Total	4510.97	2.25e6	2.29e6	2.33e5

It should be noted that the impacts of PTO operation and the motion of trapped water on the OE35 model are not considered in the analysis. This exclusion is justified based on internal tank testing conducted by OE (OE35 developer), which demonstrated that the effects of these two factors are minimal. These findings validate the assumptions underpinning the hydrodynamic model of the OE35, which is conceptualized as a barge. This model assumes a large body of water entrapped within the structure, effectively acting as ballast and stabilizing the platform under various sea conditions. This approach ensures that the model remains focused on the most significant factors affecting the platform's mooring system, while determining that the omitted factors do not substantially alter the outcomes.

2.4.2. Mooring system modelling

Shown in Fig. 5, the mooring system of the device employs a three-line catenary configuration. Specifically, Line 1 is oriented 50 degrees off the forward starboard corner, and Line 2 is similarly positioned 50 degrees off the forward port corner. Line 3, which serves as the aft line, is attached via a bridle to the aft skeg of the device. This configuration of the three lines is uniform across each, incorporating a combination of materials including nylon, chain, and polyester. The purpose of this material diversity is to provide a nonlinear mooring stiffness, which is essential for accommodating varying dynamic loads. Additionally, this setup aims to reduce tensile loading, enhancing the structural integrity and operational stability of the mooring system under diverse marine conditions. This design approach facilitates a balance between flexibility and strength, crucial for the effective functioning of the device in its marine environment.

Each single mooring line (see Fig. 6) consists of several key components that work together to ensure the stability and functionality of the OE35 in an extreme environment. The system begins with an anchor that is securely fixed to the seabed, providing the foundational stability necessary for the rest of the mooring components. Attached to this anchor is a studded bottom chain, which lies flat on the seabed. The studded design of this chain adds additional weight and stability,

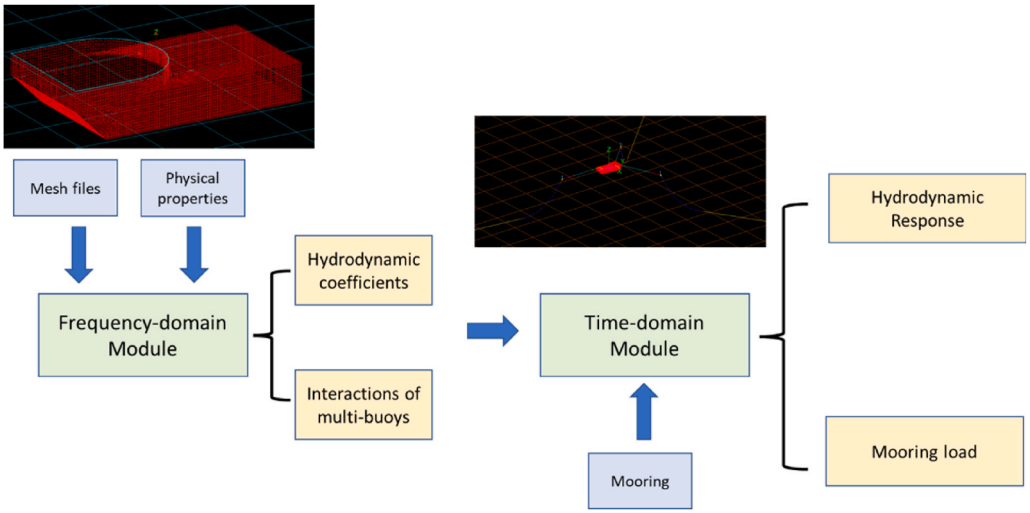

Fig. 4. Process of the Orcaflex simulation.

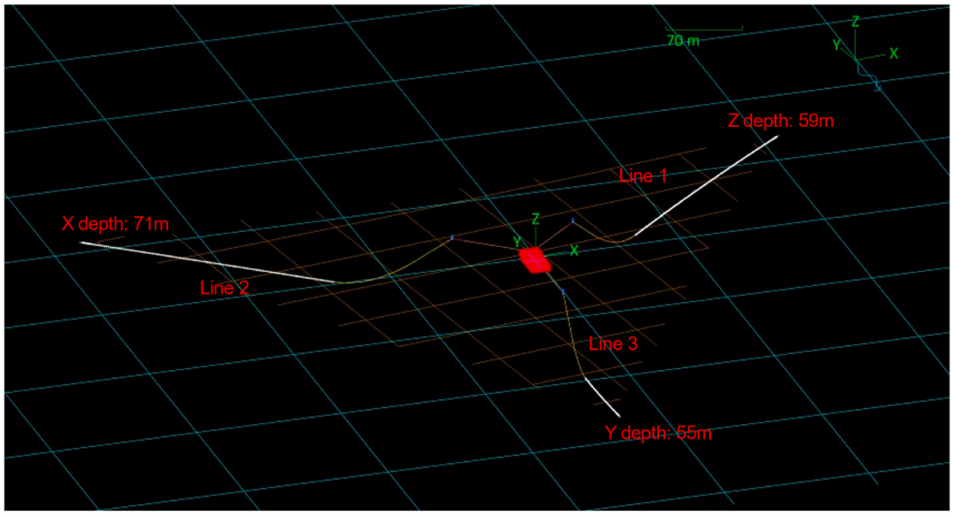

Fig. 5. Mooring configuration in Orcaflex.

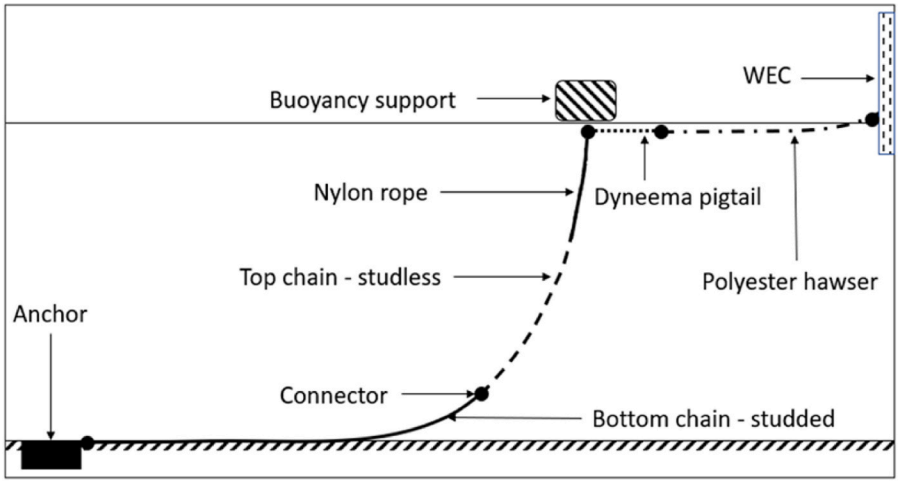

Fig. 6. Mooring line type and connectors for the OE35 mooring system.

preventing the system from shifting due to underwater currents and wave action. Connected to the bottom chain via a connector is a studless top chain. The studless design of this chain makes it lighter and more flexible, allowing it to ascend from the seabed towards the surface without compromising the system's integrity. As the mooring line continues upwards, it transitions to a nylon rope. The nylon rope is chosen for its lightweight and strong properties, as well as its elasticity, which helps absorb dynamic loads caused by wave. Midway through the mooring line, a buoyancy support is attached. This buoyant component provides an upward force, helping to keep the mooring line floating and reducing the load on the lower sections of the system. Following the nylon rope is a Dyneema pigtail, made from a high-strength synthetic fibre. The Dyneema pigtail serves as a flexible, strong, and lightweight connection between the nylon rope and the polyester hawser.

The polyester hawser, a robust synthetic rope, is utilized in the upper portion of the mooring line, ensuring a secure connection between the Dyneema pigtail and the device. This design is based on the installation process of the OE35 prototype. In future sea trials, the mooring system will be configured first, followed by the towing ship positioning the OE35 at the designated location and finally connecting the polyester hawser and Dyneema pigtail. This design facilitates easy deployment of the prototype due to the lightweight nature of the Dyneema pigtail and polyester hawser.

The specific dimensions and characteristics (see Tables 4 and 5) of above components are sourced from industry-standard product catalogues, such as the Sotra Catalogue (Chain, 2021). A key element in the design process involves applying a safety factor (1.67) to the peak tension values derived from simulation data. Consequently, the MBL of each component must surpass this adjusted tension value to ensure reliability and safety. While the dimensions of the individual components remain

Table 4
Mooring line design loads, design loads and MBL considered for simulations.

		Length [m]	Diameter [mm]	MBL [kN]
Line 1&2	Polyester Gamma98 rope	55	125	4415
	Dyneema LankoForce rope	12.2	80	4510
	Braidline DOUBLE BRAID 32/64	45	160	5758
	Studless chain Grade 3	50	78	4500
	Studlink chain Grade 2	295	90	4090
Line 3	Polyester Gamma98 rope	55	125	4415
	Dyneema LankoForce rope	12.2	80	4510
	Braidline DOUBLE BRAID 32/64	40	160	5758
	Studless chain Grade 3	50	78	4500
	Studlink chain Grade 2	99	90	4090

Table 5
Characteristics of supporting buoy.

Name and model (example)	Mobilis AMR 17000–300t
Weight [t]	4.79
Buoyancy [t]	17
Diameter [m]	4
Height [m]	5.3
Draught [m]	1.9

constant, the lengths of the sections may be adjusted throughout the iterative design process. This flexibility in adjusting section lengths is critical for managing and minimizing the loads to acceptable levels, thereby enhancing the overall efficiency of the design iterations. Notably, this approach also expedites the turnaround time between each iteration, allowing for quicker refinement and testing of the mooring system.

For example, in the case of chains, the MBL is directly associated with the grade of the chain. This means that different chain strengths can be utilized without altering the diameter of the chain, thus maintaining the integrity of the system while exploring different strength options. However, it is important to recognize that higher-grade chains, while offering increased strength, also come with higher costs and may have limited availability. Thus, the iterative design process is not solely focused on reducing peak mooring tension but also involves a careful evaluation of the cost implications associated with different component options. This balanced approach ensures that the mooring system is both effective and economically viable.

2.5. Tank test

The tank test is critical in ensuring the reliability and effectiveness of the mooring design in real ocean environments. To verify the results of the Orcaflex simulation, a scaled physical tank test of the proposed mooring system was conducted. This test was designed based on the Froude similarity principle with a scaling ratio of 1:30. The specific wave conditions tested were those defined under DLC6.1. The test was performed in the deep ocean wave tank at the LIR National Ocean Test Facility, located at University College Cork, Ireland. This testing was funded through the SEAI Industry Access Programme (Network, 2024). The related facility is equipped to replicate wave conditions accurately, providing a controlled environment to test and validate the mooring system's response under specific conditions before actual deployment.

2.5.1. Test wave conditions

In the Orcaflex simulation, DLC6.1 (Hs, of 12.93m and Tp, of 15s) was simulated over a full-scale equivalent of 3 h. However, replicating such an extended sea state in the tank environment presents practical challenges, particularly with a 30 ratio, which would equate to approximately 32.8 min. Problems such as the buildup of reflections within the tank can distort the results, making longer test durations unfeasible. To effectively validate the Orcaflex modelling within the constraints of the wave tank, a critical segment from the Orcaflex-generated 3-h wave time history was selected. This segment, designated as DLC6.1_1, captures the period around the occurrence of the peak wave height, which is responsible for the maximum force exerted during the simulation (shown in Fig. 7). This portion was chosen to correspond to a tank-scaled test duration of about 256 s, making it manageable within the tank's operational parameters. The selected section from the Orcaflex data was reproduced in the tank using wave paddles, and the new surface elevation at the location of the scaled model was measured with wave probes. This measured time history was then scaled rerun in Orcaflex as the input wave conditions to compare the tank results with the original Orcaflex simulations. In the simulation, the OE35 was oriented at 82.5° within the Orcaflex global coordinate system. Consequently, to ensure that the waves directly approached the device, the wave direction was set to 262.5° (see Fig. 8).

While the tank tests included several scenarios to investigate different aspects of the model's performance, such as PTO energy absorption, these were not the focus of this paper. The primary objective remained the validation of the Orcaflex results using the DLC6.1_1 segment, ensuring that the modelling accurately reflects the physical behaviours observed during the scaled tank tests. This focused approach helps streamline the validation process and provides a robust comparison between theoretical predictions and empirical observations.

2.5.2. OE35 scaled model

The OE35 scaled model (see Fig. 9) was constructed using 2 mm aluminium sheet, chosen for its balance of strength and lightness suitable for accurate scale modelling. The objective for the model was to achieve a target weight specified in Table 3, which represents the scaled total device weight. To ensure the scaled model reflects the hydrodynamic properties of the full-scale device, the initial lightship weight of the model was kept below this target. This design approach allowed for subsequent adjustments through the strategic placement of lump weights around the model's hull.

These adjustments were meticulously made to align the model's draft, trim, moments of inertia, and total mass with those of the full-scale

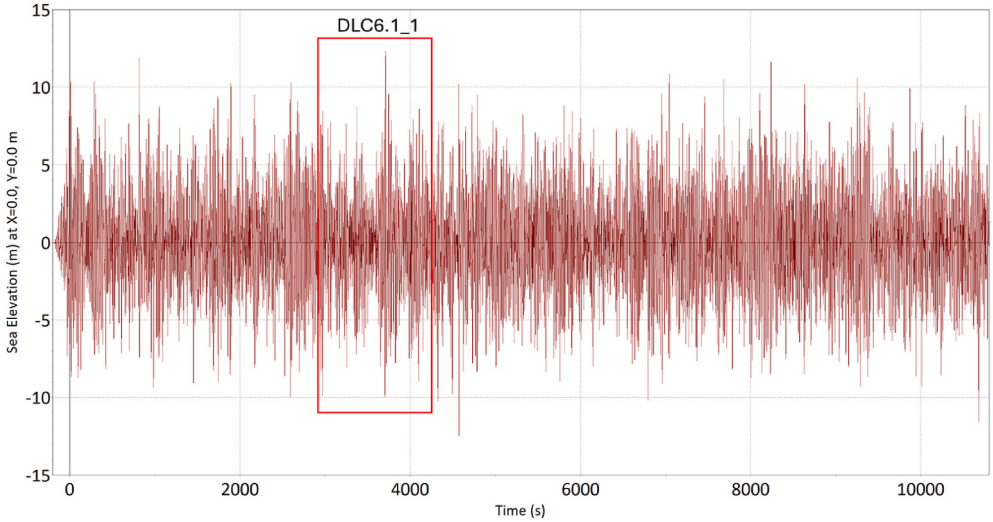

Fig. 7. DLC61_1 Surface Elevation in the simulations (unscaled).

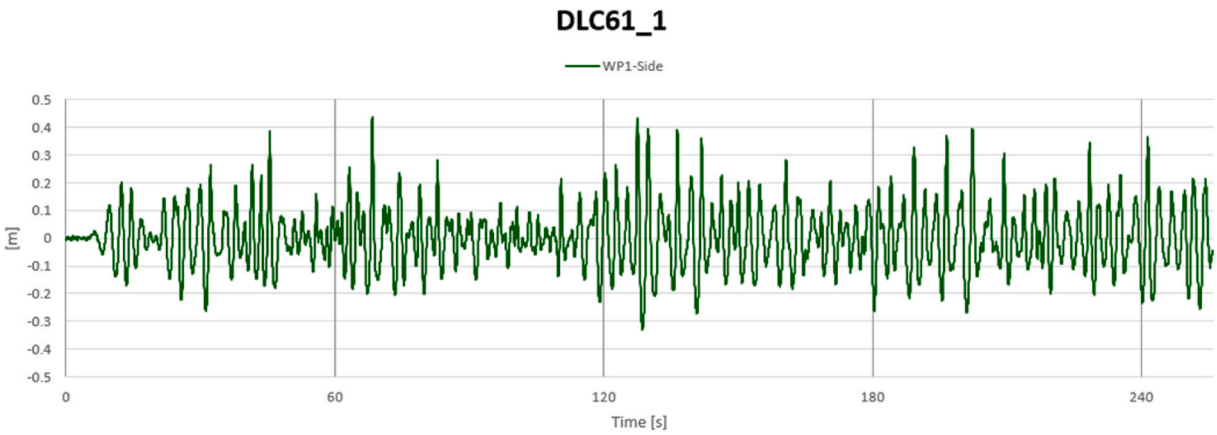

Fig. 8. DLC61_1 Surface Elevation in the tank test.

Fig. 9. OE35 scaled model.

device. The effectiveness of these modifications was validated by several key measurements: determining the Centre of Gravity, calculating the RAOs, and verifying the draft. This method ensures that the scaled model not only meets its targeted mass but also behaves in water in a manner that closely mimics the real OE35 under operational conditions.

2.5.3. *Mooring system equivalent*

Due to the limitations imposed by the width of the test tank, a direct scaled representation of each component in the mooring system was not feasible for the tank test of the OE35 model. Consequently, an equivalent method was employed to achieve the same horizontal mooring stiffness as the three-line mooring system simulated in Orcaflex, while adhering to the scaled ratio. This method involved using three mooring lines, each designed to replicate the complete mooring line from the anchor point to the device connection point. This replication was achieved by integrating a series of springs with various stiffnesses, accompanied by length-limiting stoppers on the individual springs. This setup was designed to emulate the full-scale mooring line's mechanical properties.

The process began with determining the load-extension curve of the mooring line from Orcaflex. This was done by offsetting the device along the mooring line and plotting the resulting displacement against the horizontal force at the connection point, as illustrated in Fig. 10. To accurately replicate the mooring line stiffness in the scaled model, a second curve was fitted to the Orcaflex data using spring stiffness characteristics obtained from the spring manufacturer's data sheets. The combination of these springs in series was tailored to match the complete mooring line stiffness. This calibrated approach is depicted in Fig. 11, where the Line 1 (L1) Horizontal Force reflects data from the Orcaflex model. The 'Original Fit' line represents a mathematical fit to this data, and the 'OE Fit' line shows the combined stiffness of the series

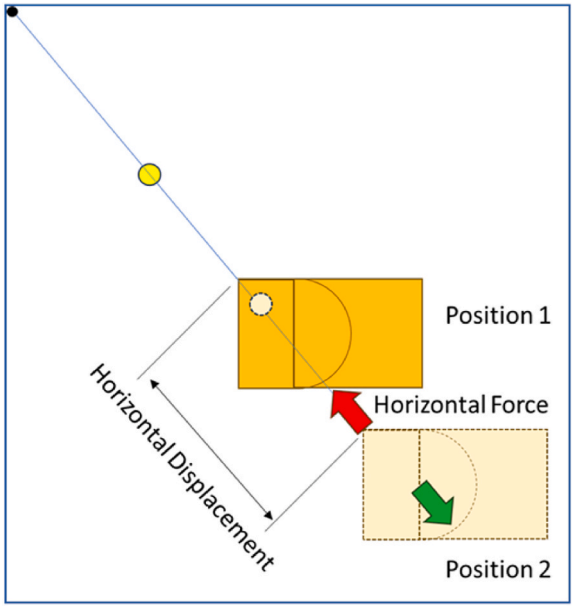

Fig. 10. Displacement of OE35 Mesh in Orcaflex to fit Springs.

springs, as determined from the manufacture's data sheets. Given the symmetry of the forward lines, Line 2 was configured identically to Line 1. The same methodology was then applied to the back line, Line 3, ensuring comprehensive replication of the original mooring system's characteristics within the constraints of the tank test environment.

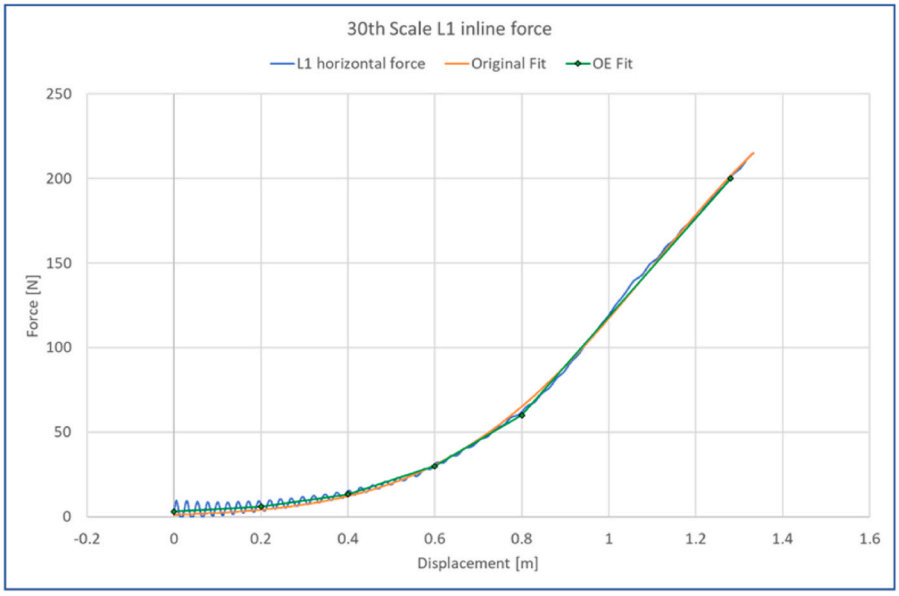

Fig. 11. Force extension curve fit.

Considering that the approaching wave is directed toward the OE35, the subsequent section—Results and Discussion—will concentrate on the mooring lines subjected to high loading, specifically Line 1 and Line 2.

To validate the spring combination setup used in the scaled mooring system model, thorough testing was conducted to ensure the setup could accurately replicate the correct extension curve. This step was essential because springs exhibit inherent properties like initial tension, which must be overcome for extension, and they may not always align perfectly with the values specified in datasheets due to variations in the manufacturing process. The testing procedure involved suspending weights from the series of springs and measuring the resulting extension. This experimental approach aimed to derive a more realistic extension plot, accounting for any discrepancies between theoretical and actual spring behaviour. These measurements are depicted in Fig. 12, where the physical setup of the spring series is shown along with the method of hanging weights for testing.

Fig. 13 compares the results from the physical tests (the unloading and loading curves) against the theoretical extension curves for the port and starboard lines, which were based on the combined stiffness of the springs. These pre-test lines represent the theoretical extension curves for the port and starboard lines based on the stiffness combination of the springs. A close examination of Fig. 13 reveals that the physical checks (unloading and loading curves) closely align with the Orcaflex data, indicating a successful replication of the mooring line behaviour in the scaled model. Fig. 13 presents the force-displacement relationship for the mooring system under different loading and unloading conditions for both the port and starboard (Stbd) sides of the device. The Target curve (red) represents the expected stiffness behaviour based on theoretical or design values, while the other curves correspond to experimental results from pre-testing and mooring line evaluations.

- Loading Process: The curves labelled “port mooring line loading” and “Stbd mooring line loading” represent the step-by-step increase in applied force as displacement increases.
- Unloading Process: The curves labelled “port mooring line unloading” and “Stbd mooring line unloading” depict the gradual reduction in force as the mooring system returns to its initial state after reaching maximum displacement.
- Pre-Testing Results: The “Pre Testing - Port” (green) and “Pre Testing - Stbd” (blue) curves correspond to preliminary tests conducted to characterize the stiffness response of each mooring line before further validation.

The results indicate a successful replication of the mooring line

Fig. 12. Setup of Spring Combinations for Mooring Line testing.

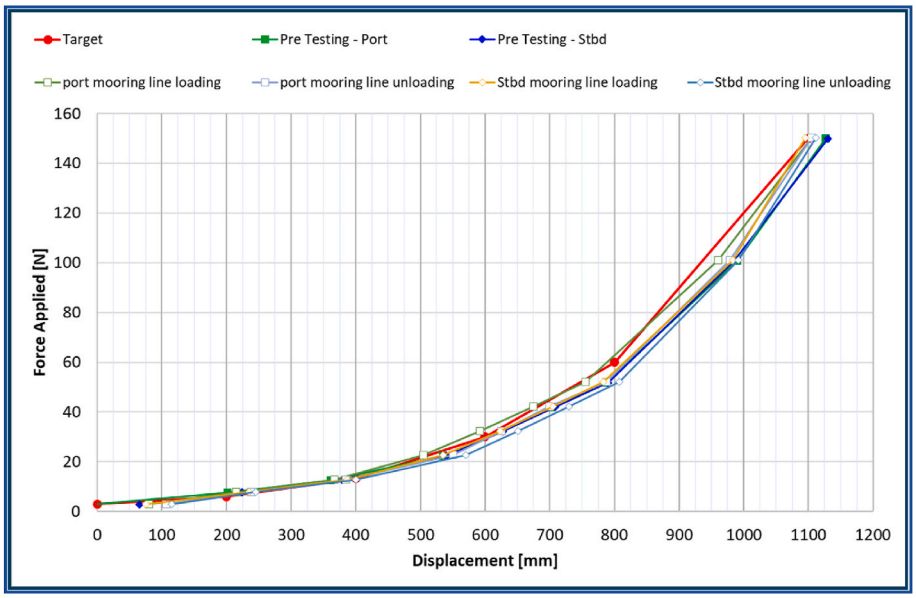

Fig. 13. Plot of spring combination force extension curves.

behaviour in the scaled model and this "good fit" confirms that the spring combination setup effectively simulates the desired characteristics of the mooring system, despite potential variances in spring performance due to manufacturing inconsistencies. This methodological approach ensures the scaled mooring system accurately reflects the mechanical properties necessary for comprehensive testing and validation of the OE35's mooring configuration.

Test layout.

Fig. 14 illustrates the plan view of the tank test setup. Point A represents the location of the actual scaled anchor point. As described earlier, springs are utilized in the setup to reduce the mooring footprint while preserving the stiffness characteristics of the mooring configuration. The mooring lines are connected horizontally to point A′, which is located at the side walls of the wave tank. The two forward mooring lines consist of a combination of springs and a force transducer, which is used to measure the force exerted on the line. Additionally, a small float is incorporated to counterbalance the weight of the springs, ensuring that the mooring lines remain as horizontal as possible. The back line also includes springs to replicate its stiffness, and it is adjusted to achieve the desired pretension as determined by the Orcaflex model. To calibrate the wave conditions in the tank, a set of wave probes (WP4-WP8) is positioned forward of the device. Another wave probe (WP1) is placed to the side of the device to approximate the wave conditions at the device's location. This setup ensures that the mooring system's behaviour is accurately modelled and that the forces and tensions in the mooring lines can be precisely measured. The use of springs and floats effectively mimics the stiffness and tension characteristics of the full-scale mooring system, allowing for a reliable validation of the Orcaflex simulation results under controlled tank test conditions.

Each forward mooring line is equipped with a force transducer to measure inline force. The plenum chamber's pressure is monitored by a pressure transducer. Reflective markers are placed on the device to capture 3D motions using the Qualysis camera system. Data capture is synchronized with the wave paddles' start, processed at 32Hz.

3. Results and discussions

3.1. Comparison with orcaflex simulation

As discussed in the previous section, the wave elevation data recorded by WP1 is transmitted to Orcaflex to replicate the wave conditions observed during the tank test. Fig. 15 shows good alignment between the peaks and troughs of both the simulation and tank test data (scaled), which indicates that the simulation scaled model behaves in a manner consistent with the simulated predictions under similar conditions.

The initial investigation involved comparing surge results from Orcaflex simulations with those from the tank test. Fig. 16 illustrates a commendable level of concordance between the simulated and experimental outcomes, attesting to the simulation's ability to accurately mirror real-world dynamics. These findings affirm the robustness of the Orcaflex model and its capacity to intricately capture the complex responses of the OE35 to wave forces. Although there are some variances between the two data sets, such discrepancies are anticipated and serve as crucial indicators for areas where the simulation parameters may be further refined to enhance predictive accuracy and reliability. Further investigate the system's dynamic response, additional degrees of freedom have been analysed under DLC6.11. Figs. 17 and 18 illustrate the heave and pitch motion comparisons between Orcaflex simulations and tank tests. The results also show good agreement in the overall trends, demonstrating that the numerical model effectively predicts the motion behaviour of the OE35.

Fig. 19 illustrates the comparison of force at the device connection point between the Orcaflex simulation and the tank trials for DLC6.1_1. The graph reveals that the peak force in the simulation exceeds twice the magnitude of that measured in the tank trials, pointing to significant discrepancies in the results. Upon investigation, two main factors have been identified that might account for these differences.

Firstly, the dynamic effect of the mooring buoy floats, especially when fully submerged, was not modelled in the tank trials. The floater in the tank is used to keep the spring horizontal rather than lift the mooring line like the mooring buoy in the full scaled mooring configuration. While initially considered a minor omission, it was concluded that this alone could not induce such a large difference in the force measurements.

Secondly, and more critically, the simulation included the situation of the mooring lines are fully extended which caused by the fixed anchor point. This scenario results in a sharp increase in tension, which was not replicated in the tank trials (the individual spring will be limited by the stopers). This differences in the tank setup likely led to significantly lower peak forces recorded during the trials. In practical terms, the mooring line fully extension creates a scenario where the mooring lines are subjected to abrupt and extreme tension, which does not occur in the

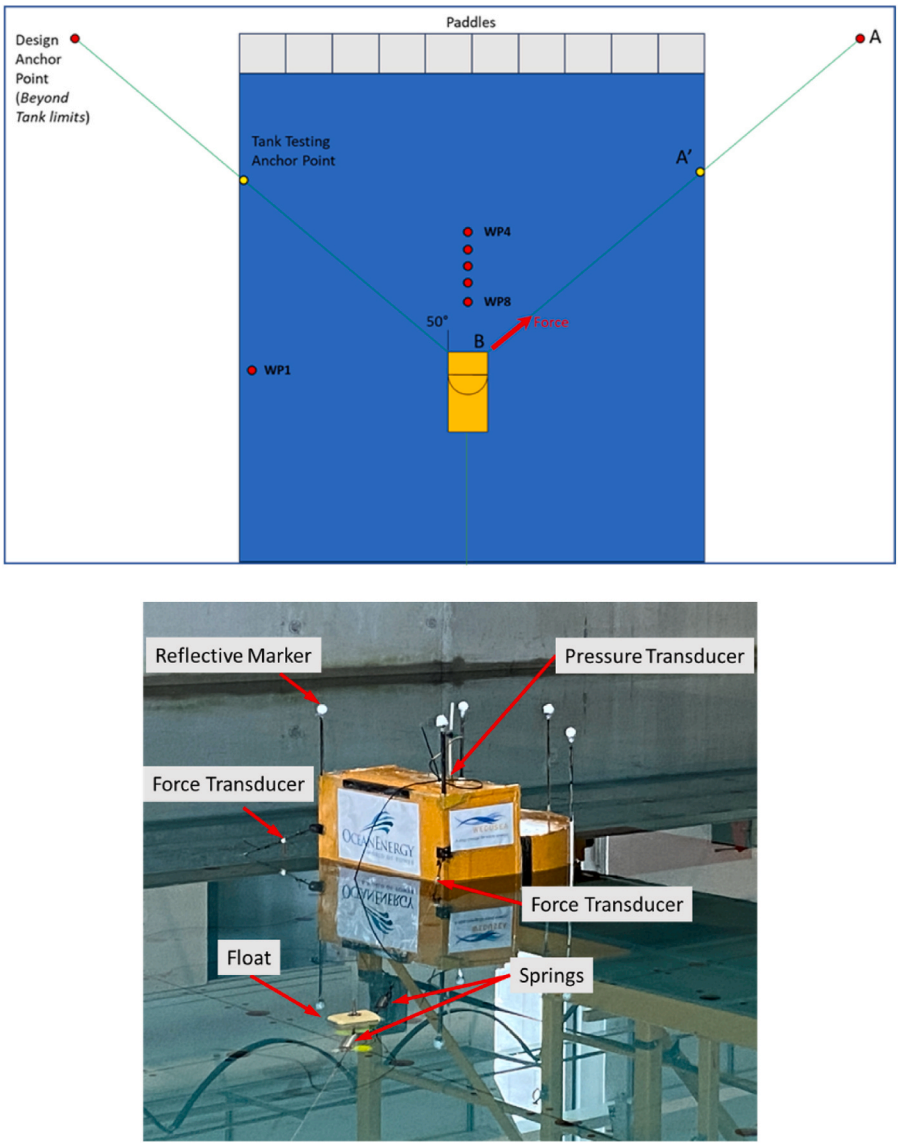

Fig. 14. Tank task layout.

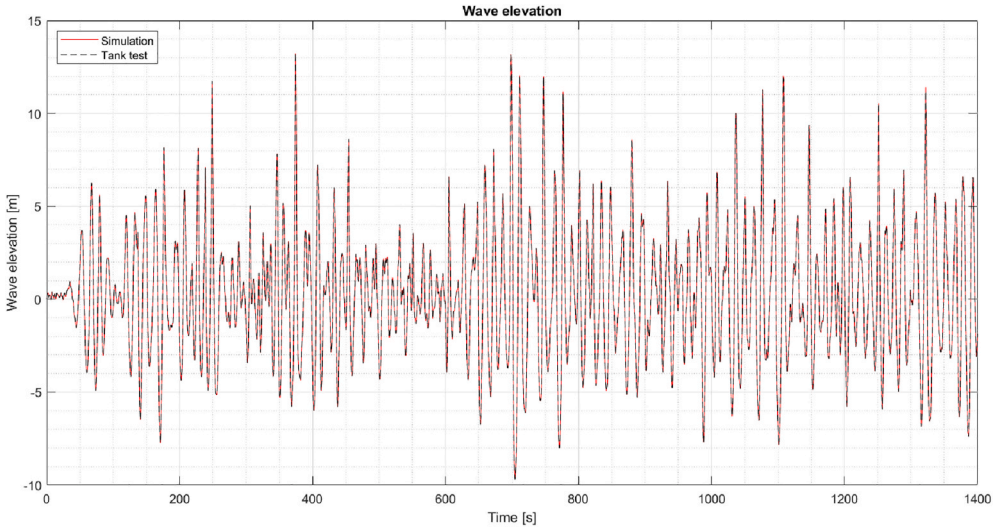

Fig. 15. Wave elevations between simulations and tank test, DLC6.1_1, the time length (256s) has been scaled into full scaled model.

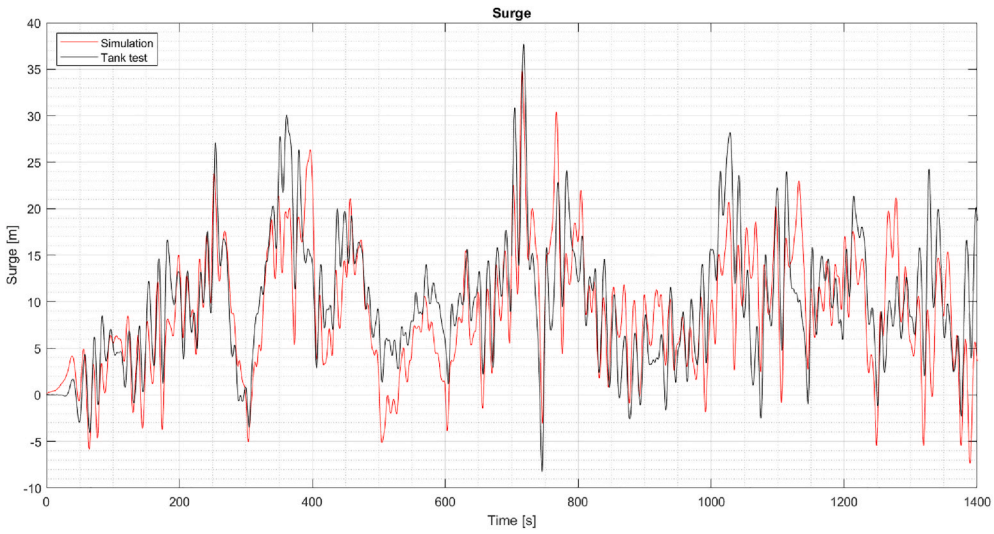

Fig. 16. Comparison of Surge motion, DLC6.1_1.

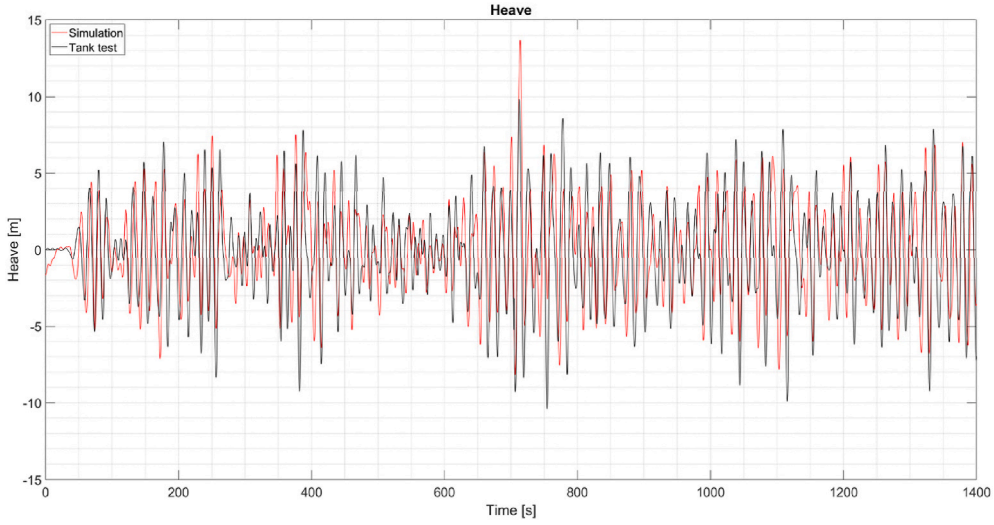

Fig. 17. Comparison of Heave motion, DLC6.1_1.

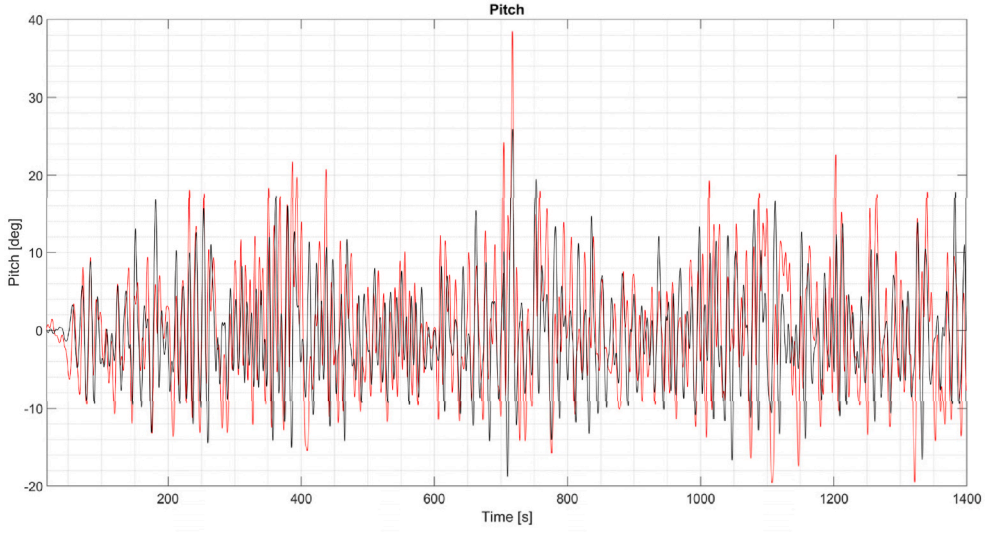

Fig. 18. Comparison of Pitch motion, DLC6.1_1.

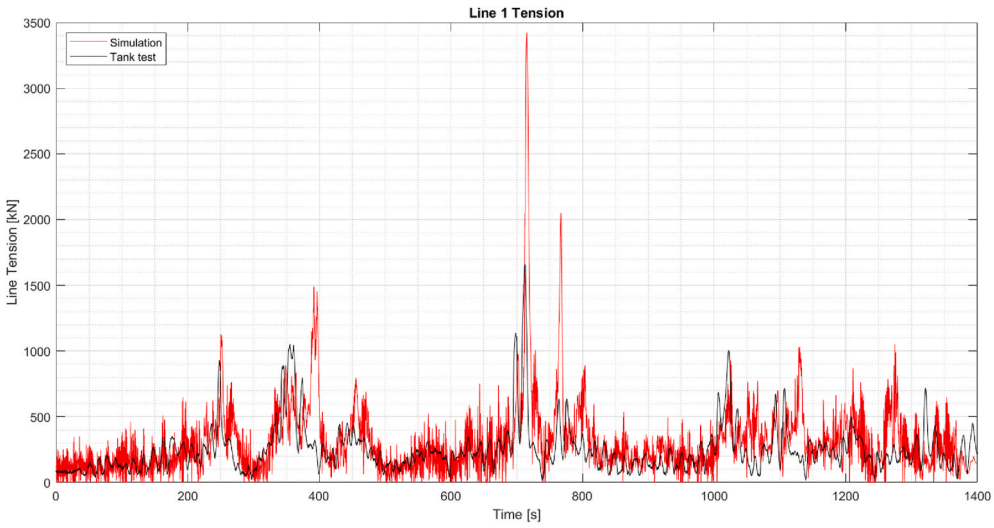

Fig. 19. Comparison of Line 1 tension, DLC6.1_1.

physical model tests, thus explaining the pronounced variation in the measured forces.

To provide a more comprehensive validation of the mooring system, additional comparisons have been included, addressing multiple sea states beyond the single extreme condition (DLC6.11). Table 6 below summarizes the sea state conditions analysed.

The comparison of maximum mooring line tension for different sea states is presented in Fig. 20. The results highlight variations between Orcaflex simulations and tank test outcomes. The largest discrepancy occurs in DLC6.11, where the simulated tension is significantly higher than that measured in the tank test. This is also due to the full lifting of the mooring line, which was not replicated in the experimental setup. In contrast, lower sea states (B08, B10, B14, and B15) show better agreement between simulations and physical tests, indicating that the mooring model in Orcaflex accurately captures system behaviour under moderate conditions.

Finally, aside from the distinct peak load discrepancies, the Orcaflex results align closely with the tank test outcomes throughout the rest of the test duration. This alignment demonstrates the accuracy of the Orcaflex simulation in capturing the dynamic behaviour of the mooring system and confirms the effectiveness of the stiffness equivalent method used in the tank test.

3.2. Simulation results

The assessment of the mooring design focused on a head sea condition defined by DLC6.1, with a Hs of 12.93 m and a of 15 s.

The results from these simulations are depicted in the time histories illustrated in Figs. 21 and 22. These figures specifically highlight the maximum tension at the fairlead adjacent to the WEC. The maximum tension for the two upwind mooring lines (Line1 and Line2 were symmetrical, so only Line 1 results were presented) was recorded at 4000 s. Compared to Fig. 7, DLC61_1 Surface Elevation in the simulations (unscaled), the occurrence of the peak force slightly lags behind the peak wave height. However, DLC 6.1_1 still successfully captures the peak occurrence. This again demonstrates the effectiveness of the wave segment selection method used in the tank test. It should be noted that the duration of the wave segment selection may vary in other projects. Therefore, readers are advised to ensure that the wave segment covers the peak force of the mooring line if a similar method is applied. Meanwhile, Line 3, representing the downwind (lee) line, exhibited its maximum tension at 2700 s, displaying lower tension characteristics in comparison to the upwind lines. The highest tension observed across all lines was $T_{max} = 2024$ kN.

Table 6
The sea state conditions (unscaled).

Sea s	Hs (m)	Tp (s)
B10	8	12.73
B08	7.5	10.61
B15	5	17.68
B14	8	14.14
DLC6.11	12.93	15

Figs. 23 and 24 display the results of the surge (OE35 Y) and sway (OE35 X) motion of the OE35. The surge motion has an offset ranging from +15 m to −25 m, while the sway motion varies between +4 m and −1.5 m. These movements meet the future sea trail requirement, which has a radius of 30 m, indicating that the WEC's motion remains within safe operational limit.

Figs. 25 and 26 present the results for the loads at the anchor points for all three anchors providing holding capacity for line 1 to 3. The simulation results show maximum anchor loads of just below 2000 kN for line 1 (2), whilst anchor loads for line 3 are just below 1200 kN. These loads were used to design and select the drag embedment anchors for the future sea trail. To ensure the effectiveness of drag embedment anchors, it is crucial that the uplift angle on the anchor remains below 5°. Fig. 27 showcase the results concerning anchor lift-off for mooring line 1, which was deployed heading to the waves. These figures reveal the behaviour of the anchor angles throughout the simulation, including the initial 'run up' phase (time steps before 0), where the anchor dynamics are established. During this phase, the mean declination angle stabilizes at approximately 88.7°. Over the course of the simulation, a slight variation in the declination angle of about ±0.8° were observed. It is important to note that a 90° declination angle corresponds to an anchor lying flat along the seabed. This scenario assumes a completely flat bathymetry, which is the standard setting used in the Orcaflex simulations to simplify the model and focus on the anchor dynamics under controlled conditions.

The selection of components for the mooring system was driven by the need to achieve a MBL that would ensure adequate holding capacity for the system. The mooring configuration under assessment experiences a peak force of 2024 kN. By applying a safety factor of 1.67 to this peak force, a required maximum strength of 3380 kN is derived to ensure safety and reliability under extreme conditions.

Given these specifications, there exists potential to optimize the system further. Specifically, the current headroom allows for the possibility of reducing the diameter of the chains and ropes used in the mooring system, contingent upon successful outcomes of subsequent

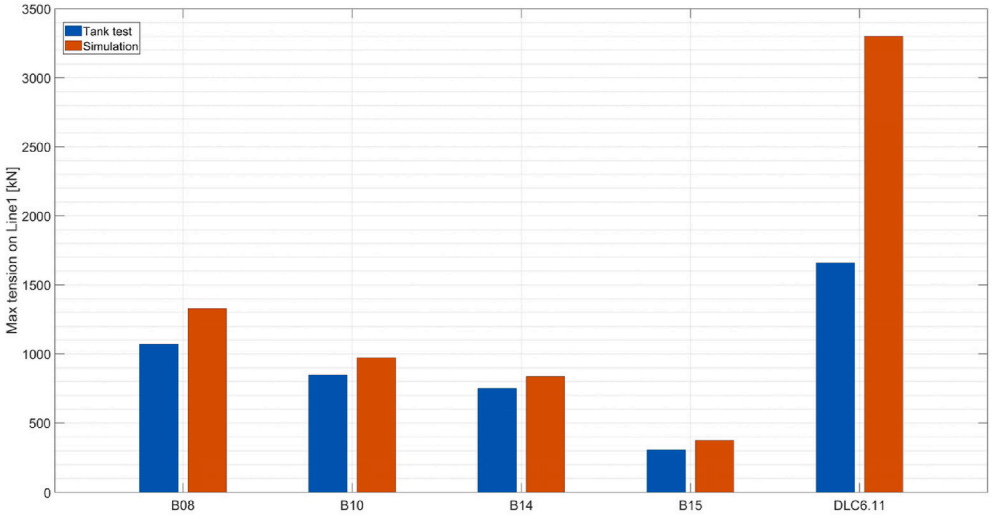

Fig. 20. Maximum mooring line tension comparison across different sea state.

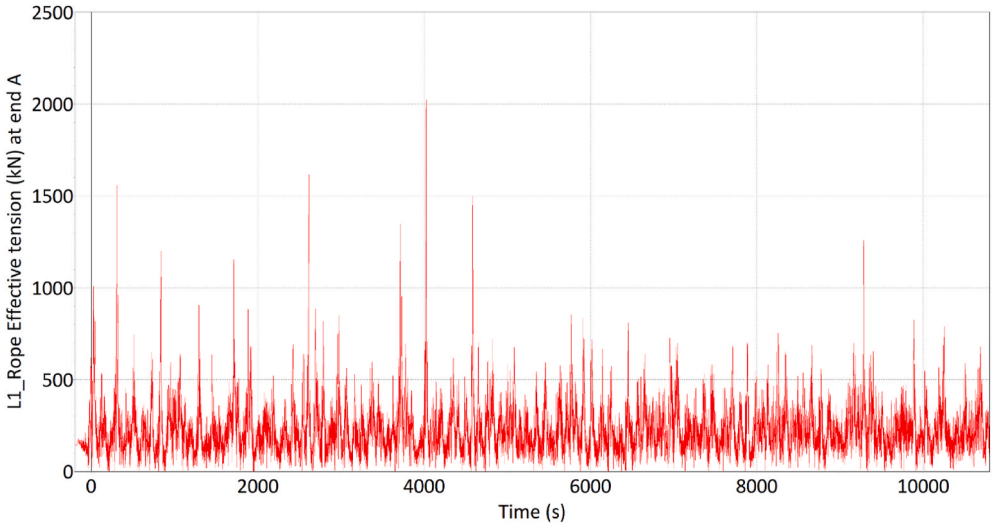

Fig. 21. Line 1 effective tension [kN] at device.

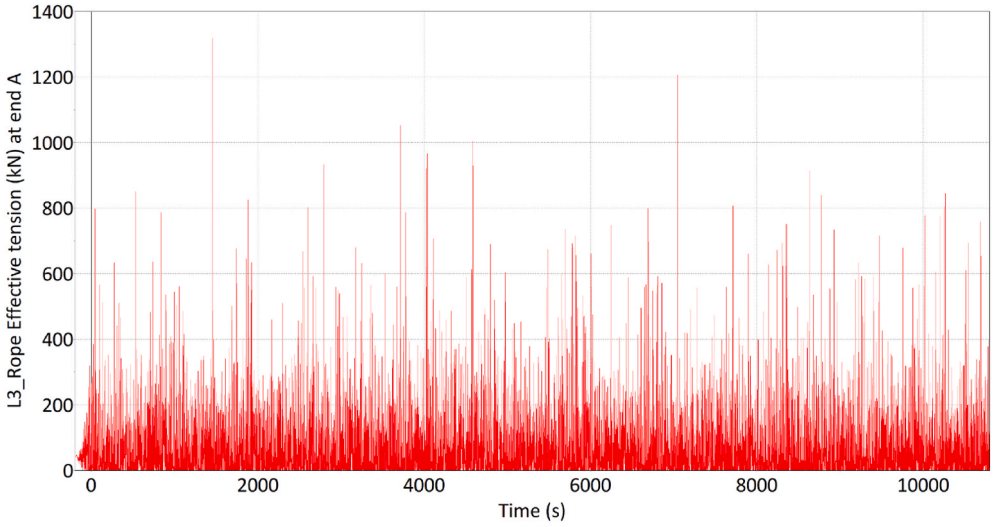

Fig. 22. Line 3 effective tension [kN] at device.

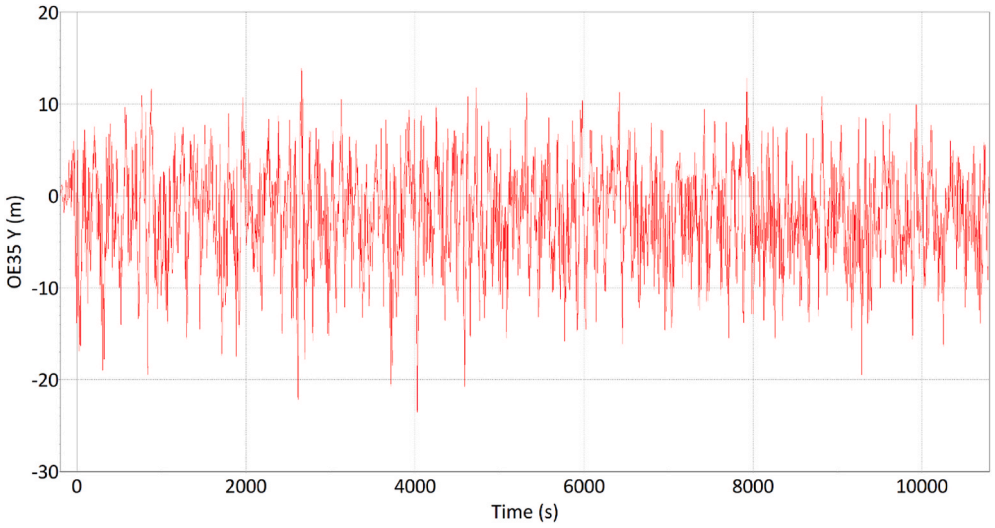

Fig. 23. OE35 surge offset.

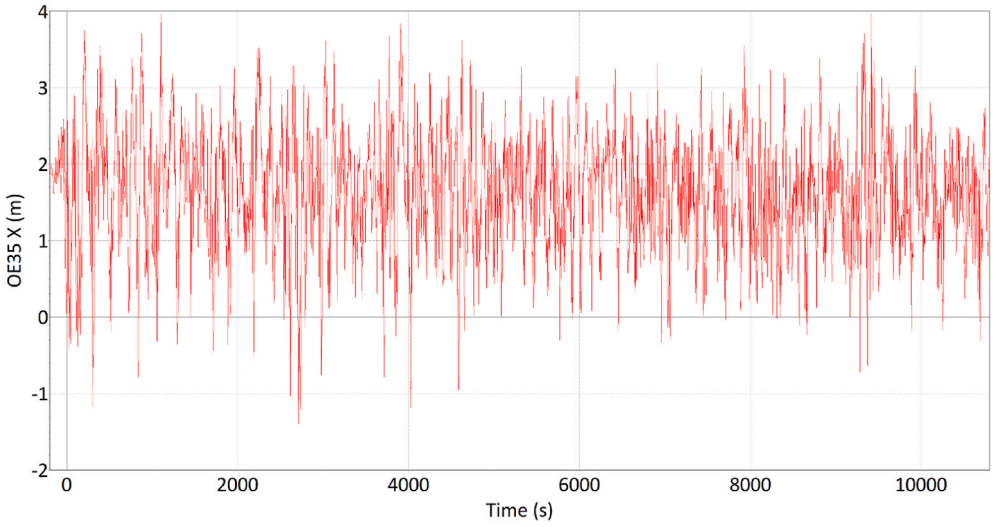

Fig. 24. OE35 sway offset.

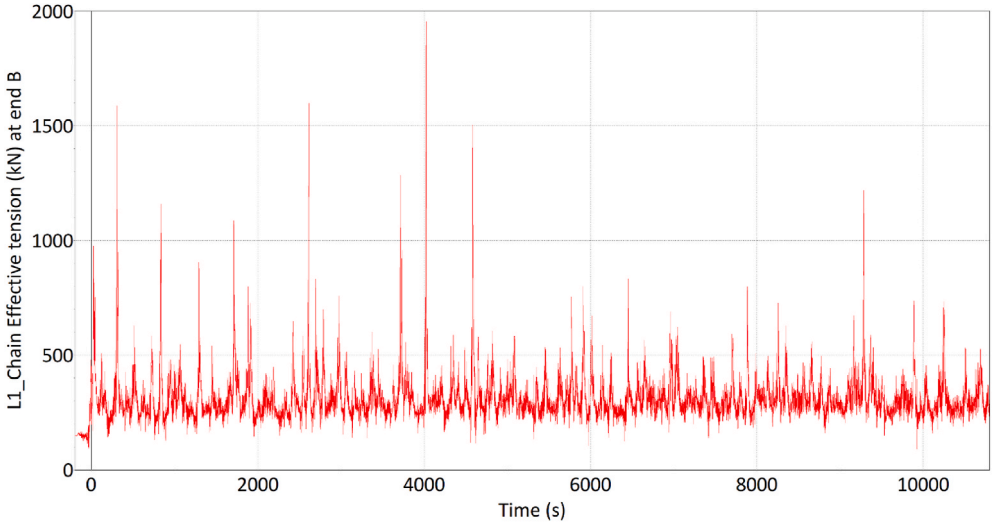

Fig. 25. Line 1 Effective Tension [kN] at Anchor point.

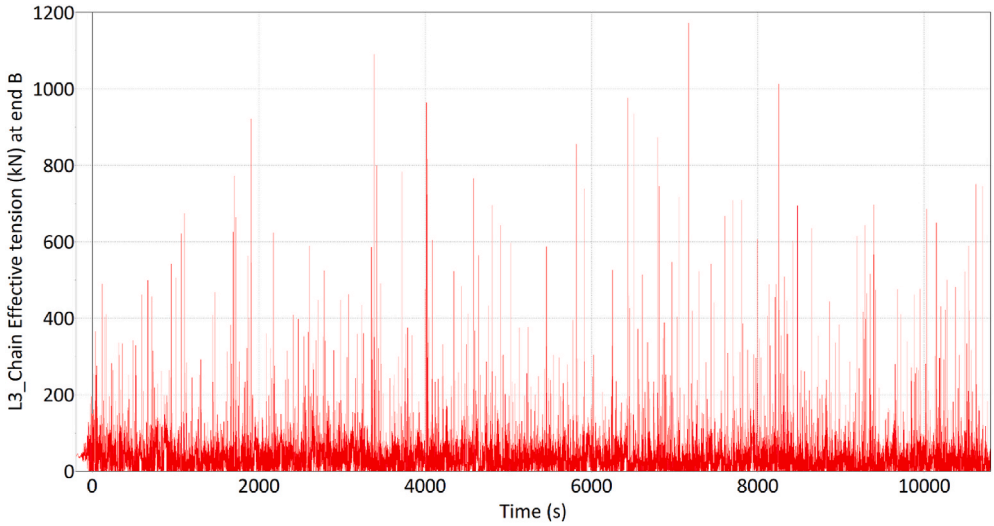

Fig. 26. Line 3 Effective Tension [kN] at Anchor point.

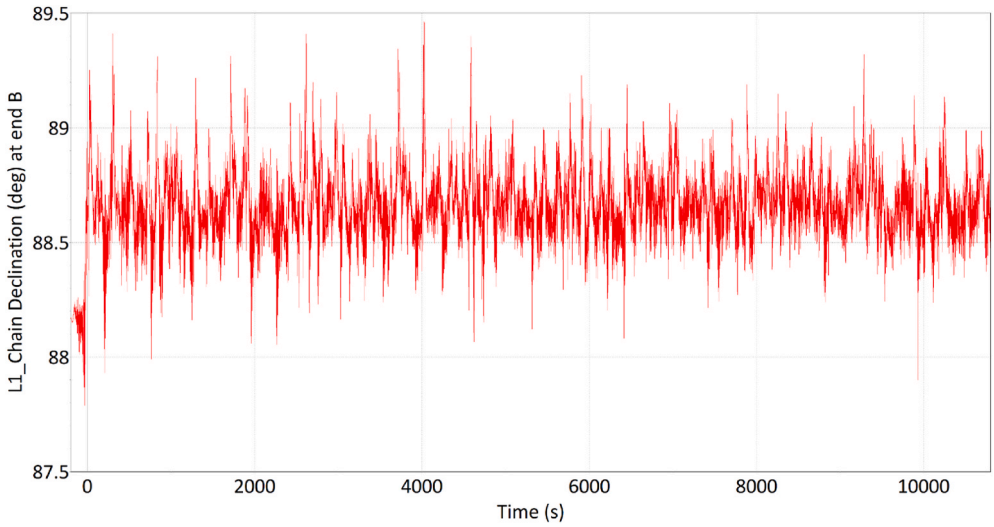

Fig. 27. Line 1 Declination Angle at anchor point.

iterative mooring validations. This optimization would not only potentially reduce costs and material usage but also enhance the efficiency of the mooring setup while maintaining the necessary safety margin.

3.3. Mooring configuration summary

This section outlines the components and configurations of the three lines used in the final mooring setup under investigation. Fig. 28 illustrates the various elements of the mooring line configuration, providing a visual representation of each component's arrangement. Additionally, the specific configurations for each of the three lines are detailed in Table 7.It is important to note that some of the information presented here may duplicate content found in Table 4. The authors have chosen to list these details again in this section to facilitate easy reference and verification for readers, ensuring clarity and convenience in understanding the mooring setup.

It should be noted that the Working Load Limit (WLL) for the shackle already includes a substantial safety factor, typically around 3 to 4

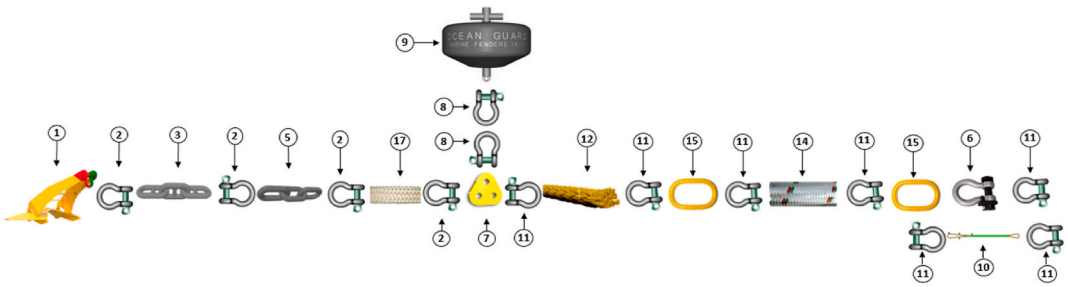

Fig. 28. Mooring components of the catenary system.

Table 7
Line elements, condition monitoring equipment and mooring connectors for front mooring lines.

Ref. No	Component name	Properties	Number	Length [m]	Comment
1	Anchor	Based on simulation	1	NA	
2	Bow shackle	WLL 2000 kN	4	NA	Suitable for 90 mm studded chain
3	Bottom chain	MBL: 4090 kN, Studded Grade 2	1	295 for front lines, 99 for the back line	90 mm diameter needed for weight
5	Top chain	MBL: 4500 kN, 78 mm studless Grade 3	1	50	78 mm diameter needed for weight
6	Load shackle	WLL 2000 kN	2	NA	Measurement range based on the expected maximum loads
7	Triplate	WLL 2000 kN	1	NA	For connection of nylon rope shackle, buoy shackle and Dyneema shackle
8	Bow shackle	WLL 2000 kN	2	NA	Suitable for connection to supporting buoy
9	Supporting buoy	Detailed in Table 5	1	NA	Dimensions based on the OrcaFlex model
10	Safety line	WLL 2000 kN	1	3	Redundancy line for load shackle
11	Bow shackle	WLL 2000 kN	7	NA	For connection of Dyneema pigtail to triplate and polyester hawser to load shackle
12	Pigtail	MBL 4510 kN	1	12.2	Dyneema construction e.g. Dyneema LankoForce rope
14	Hawser	MBL 4415 kN	1	55	Polyester construction e.g. Polyester Gamma98 rope
15	Master link	WLL 2000 kN	2	NA	Connection of load shackle, redundancy line, polyester hawser and dyneema pigtail
17	Nylon rope	MBL 5758 kN	1	45 for front lines and 40 for the back line	160 mm diameter

times, because it is designed as lifting equipment. As a result, shackles with a WLL of 2000 kN are considered suitable for connecting different sections of the mooring line.

3.4. Discussions

The mooring system design for the OE35 demonstrates a comprehensive approach that balances innovative design with practical considerations. This system integrates diverse materials and sectional combinations to meet the demanding conditions of marine environments. For example, nylon is utilized in the mooring lines due to its damping properties, which help to reduce the system's response to dynamic stresses induced by wave action. A critical aspect of the design process was the use of basin tests, which employed a horizontal stiffness method. This method utilized a combination of springs to replicate the mooring system's behaviour in a scaled environment, addressing the challenges posed by scaling effects and tank limitations. The successful application of this method underscores its potential adaptability to other floating structures, such as offshore wind turbines, which face even greater environmental challenges.

The results from the Orcaflex simulations, when compared with the basin test outcomes, generally align well, particularly in terms of overall dynamic behaviour. This alignment validates the accuracy of the simulation model and the effectiveness of the stiffness equivalent method used in the tank tests. However, notable discrepancies were observed in peak load measurements. These differences are primarily attributed to two factors. First, the dynamic effects of mooring buoy floats, especially when fully submerged, were not accounted for in the tank trials. Second, the absence of the consideration of mooring line fully extension in the tank setup, which is present in the simulations, leads to lower peak forces being recorded in the physical tests. This extension in simulations creates a scenario where the mooring lines experience abrupt and extreme tension, unlike in the physical model tests. Despite these discrepancies, the overall consistency between the simulation and experimental data reinforces the robustness of the mooring design approach. The current configuration of the mooring system, tested under head sea conditions defined by DLC6.1, reveals that the design can withstand significant environmental loads. The maximum tension recorded was 2024 kN and applying a safety factor of 1.67 yields a required maximum strength of 3380 kN. This indicates that there is potential to optimize the system further by reducing the diameter of chains and ropes, contingent upon successful outcomes from iterative mooring validations.

The development of this mooring system has significant implications for future sea trials at the EMEC, where the OE35 will be tested in real sea conditions. These trials will provide critical data to further validate and refine the design.

4. Conclusions

This study provides a three-stage design approach of the mooring system for the OE35, underscoring significant advancements in the mooring strategies for wave energy technologies. Employing a combination of numerical modelling with Orcaflex software and physical basin testing, the research validated a three-point catenary mooring configuration optimized to withstand severe marine environments while enhancing the operational stability and integrity of the OE35 device. The mooring design methodology was meticulously developed beginning with OrcaFlex simulations based on detailed design load cases, followed by validation through scaled physical tank tests. This iterative design process allowed for continual refinement, accommodating the dynamic stresses of extreme sea states and ensuring the system meets established criteria for both safety and functionality.

Other key findings indicate that the mooring system effectively handles extreme DLC, particularly under head sea conditions. The stiffness equivalent method used during the tank test is demonstrated to be a feasible way to replicate the scaled mooring system stiffness and address the scaling effects under the physical limitations. The validation, despite some discrepancies mainly due to non-inclusion of dynamic effects like mooring buoy floats and the mooring line full extension considerations, aligns closely with the simulation results.

Future studies should focus on refining the simulation models to incorporate more dynamic effects and exploring alternative materials and configurations to further improve the performance and durability of the mooring system. The upcoming sea trials at the EMEC will provide critical data to validate these findings in real sea conditions, offering a pivotal step towards the commercial deployment of the OE35 and potentially other similar WECs.

CRediT authorship contribution statement

Chenyu Zhao: Writing – review & editing, Writing – original draft. **Faryal Khalid:** Writing – review & editing, Methodology. **Tony Lewis:** Supervision, Project administration. **Sean Barrett:** Methodology,

Investigation. **Brian McSwiney:** Methodology, Investigation. **Rémy CR. Pascal:** Software, Resources, Methodology, Investigation. **Bernardo Kahn:** Software, Resources, Methodology, Investigation. **Lars Johanning:** Writing – review & editing.

Declaration of competing interest

The authors declare that they have no known competing financial interests or personal relationships that could have appeared to influence the work reported in this paper.

Acknowledgement

This paper was carried out in the WEDUSEA project and funded by the EU and the Innovate UK.

References

Aubault, A., Alves, M., Sarmento, A.n., Roddier, D., Peiffer, A., 2011. Modeling of an oscillating water column on the floating foundation WindFloat. In: International conference on offshore mechanics and arctic engineering.

Chain, S.A.a., 2021. Anchor and Chain Handbook, eighth ed. https://www.sotra.net/contact/order-handbook/.

Clemente, D., Rosa-Santos, P., Taveira-Pinto, F., 2021. On the potential synergies and applications of wave energy converters: a review. Renew. Sustain. Energy Rev. 135, 110162.

Commission, I.E., 2021. IEC technical specification 62600-10. https://webstore.iec.ch/en/publication/66050.

Czech, B., Bauer, P., 2012. Wave energy converter concepts: design challenges and classification. IEEE Ind. Electron. Mag. 6 (2), 4–16.

DNV, 2018. DNVGL-OS-E301. https://rules.dnv.com/docs/pdf/DNVPM/codes/docs/2013-10/OS-E301.pdf#:~:text=We%20would%20like%20to%20show%20you%20a%20description%20here%20but.

EMEC, 2023. Emec demonstration – OE35. https://www.emec.org.uk/about-us/wave-clients/oceanenergy/.

Freeman, K., Dai, M., Sutton, R., 2014. Control strategies for oscillating water column wave energy converters. Underw. Technol. 32 (1), 3–13.

Gomes, R.P., Henriques, J., Gato, L., Falcao, A.d.O., 2011. Design of a floating oscillating water column for wave energy conversion. Proc. 9th Eur. Wave Tidal Energy Conf. Southampton, UK.

Gubesch, E., Abdussamie, N., Penesis, I., Chin, C., 2022. Effects of mooring configurations on the hydrodynamic performance of a floating offshore oscillating water column wave energy converter. Renew. Sustain. Energy Rev. 166, 112643.

INNOSEA, 2022. WED-T2.6-INNO-N07-1x6_resourceCodeDataAnalysis_point250070.pdf.

Jin, S., Greaves, D., 2021. Wave energy in the UK: status review and future perspectives. Renew. Sustain. Energy Rev. 143, 110932.

Johanning, T.L.L., 2023. WEDUSEA: creating a step change for the wave energy industry. https://ore.exeter.ac.uk/repository/bitstream/handle/10871/132813/V18N1+essay+Lewis+and+Johanning+LR.pdf?sequence=1.

Khaleghi, S., Lie, T.T., Baguley, C., 2022. An overview of the oscillating water column (OWC) technologies: issues and challenges. J. Basic Appl. Sci. 18, 98–118.

Kisacik, D., Stratigaki, V., Wu, M., Cappietti, L., Simonetti, I., Troch, P., Crespo, A., Altomare, C., Domínguez, J., Hall, M., 2020. Efficiency and survivability of a floating oscillating water column wave energy converter moored to the seabed: an overview of the EsflOWC MaRINET2 database. Water 12 (4), 992.

Kushwah, S., 2021. An oscillating water column (OWC): the wave energy converter. J. Inst. Eng.: Series C 102 (5), 1311–1317.

M'zoughi, F., Aboutalebi, P., Garrido, I., Garrido, A.J., De La Sen, M., 2021. Complementary airflow control of oscillating water columns for floating offshore wind turbine stabilization. Mathematics 9 (12), 1364.

Network, M.I.I., 2024. https://marine-ireland.ie/node/1380.

OceanEnergy, 2024. OceanEnergy. https://oceanenergy.ie/.

Orcina, 2024. Orcaflex. https://www.orcina.com/orcaflex/.

Pols, A., Gubesch, E., Abdussamie, N., Penesis, I., Chin, C., 2021. Mooring analysis of a floating OWC wave energy converter. J. Mar. Sci. Eng. 9 (2), 228.

Vannucchi, V., Cappietti, L., 2016. Wave energy assessment and performance estimation of state of the art wave energy converters in Italian hotspots. Sustainability 8 (12), 1300.

Wang, W., Zhao, C., Peng, W., Ding, W., Chen, M., Li, Y., Johanning, L., 2022. Nonlinear mooring system for a 'Sharp-Eagle'wave energy converter. Ocean Eng. 260, 111970.

Xu, S., Rezanejad, K., Gadelho, J., Wang, S., Soares, C.G., 2020. Experimental investigation on a dual chamber floating oscillating water column moored by flexible mooring systems. Ocean Eng. 216, 108083.

Zhao, C., Stansby, P., Johanning, L., 2023. OrcaFlex predictions for a multi-float hinged WEC with nonlinear mooring systems: elastic mooring force and dynamic motion. Ocean Eng. 286, 115504.

Zhou, Y., Ning, D., Shi, W., Johanning, L., Liang, D., 2020. Hydrodynamic investigation on an OWC wave energy converter integrated into an offshore wind turbine monopile. Coast. Eng. 162, 103731.